Melatonin restores osteoporosis-impaired osteogenic potential of bone marrow mesenchymal stem cells and alleviates bone loss through the *HGF/PTEN/Wnt/* β-catenin axis

Jun Zhang, Guoliang Jia, Pan Xue and Zhengwei Li iD

Abstract

Background: Previous studies reported that melatonin exerts its effect on mesenchymal stem cell (MSC) survival and differentiation into osteogenic and adipogenic lineage. In the current study we aimed to explore the effect of melatonin on osteoporosis and relevant mechanisms.
Methods: Real-time qualitative polymerase chain reaction (RT-qPCR) and Western blot analysis were conducted to determine expression of *HGF, PTEN*, and osteoblast differentiation-related genes in ovariectomy (OVX)-induced osteoporosis mice and the isolated bone marrow MSCs (BMSCs). Pre-conditioning with melatonin (1 µmol/l, 10 µmol/l and 100 µmol/l) was carried out in OVX mice BMSCs. Bone microstructure was analyzed using micro-computed tomography and the contents of alkaline phosphatase (ALP) and tartrate-resistant acid phosphatase 5b (TRAP5b) were detected by enzyme-linked immunosorbent assay in serum. BMSC proliferation was measured by cell-counting kit (CCK)-8 assay. Alizarin red S (ARS) staining and ALP activity assay were performed to assess BMSC mineralization and calcification. The activity of the *Wnt*/β-catenin pathway was evaluated by dual-luciferase reporter assay.
Results: Melatonin prevented bone loss in OVX mice. Melatonin increased ALP expression and reduced TRAP5b expression. *HGF* and β-catenin were downregulated, while *PTEN* was upregulated in the femur of OVX mice. Melatonin elevated *HGF* expression and then stimulated BMSC proliferation and osteogenic differentiation. Additionally, *HGF* diminished the expression of *PTEN*, resulting in activated *Wnt*/β-catenin pathway both *in vitro* and *in vivo*. Furthermore, melatonin was shown to ameliorate osteoporosis in OVX mice *via* the *HGF/PTEN/Wnt*/β-catenin axis.
Conclusion: Melatonin could potentially enhance osteogenic differentiation of BMSCs and retard bone loss through the *HGF/PTEN/Wnt*/β-catenin axis.

Introduction

Osteoporosis is a common systemic skeletal disorder characterized by low bone mass and microarchitectural deterioration in bone tissues, resulting in bone fragility and an enhanced fracture risk.[1] Postmenopausal women are more likely than men to suffer from osteoporosis.[2] Risk factors for the disease include age, glucocorticoid use, and decreased bone mineral density (BMD).[3] The impairment of osteoblast differentiation and bone formation is also a cause of osteoporosis.[4] Mesenchymal stem cells (MSCs) have shown

Correspondence to:
Zhengwei Li
Department of Orthopedics, The Second Hospital of Jilin University, No. 218, Ziqiang Road, Changchun, Jilin Province 130041, P.R. China
lizhengwei@jlu.edu.cn

Jun Zhang
Guoliang Jia
Pan Xue
Department of Orthopedics, The Second Hospital of Jilin University, Changchun, P.R. China

crucial roles in the maintenance of the dynamic balance of bone metabolism.[5] Bone marrow MSCs (BMSCs) are capable of differentiating into mainly osteoblasts and adipocytes in bone and fat formation, whereupon a decline of BMSC differentiation into osteoblasts triggers the impaired bone formation in osteoporosis.[6] Therefore, it is useful to rule out the therapies targeting osteogenic differentiation of BMSCs for osteoporosis.

Melatonin is a ubiquitous hormone that is reported to be associated with a variety of functions such as sleep disorders, circadian rhythm regulation, anti-inflammation, anti-oxidation, anti-tumor, anti-depression, and vasodilation through its receptors.[7] Melatonin, which regulates dark signals and provides night-time information, is also considered an 'endogenous synchronizer' that stabilizes and enhances various circadian rhythms in the body.[8] It has been documented that melatonin is capable orchestrating bone mass through melatonin receptor 2 (MT2) receptors.[9] Also, melatonin has been identified as a safe and effective bone loss therapy because of its osteoblast-inducing, bone-enhancing effects and improvement in quality of life through MT2 receptors.[10] Melatonin demonstrated promoting effects on the osteogenic differentiation of BMSCs.[11] Melatonin treatment increases the number of trabecular bones, improves the microstructure of the femur and vertebra, and enhances bone mass density in osteoporosis mice.[12] Adipose tissue-derived MSCs treated with 5 μmol melatonin presented with upregulated hepatocyte growth factor (*HGF*), a key mitogenic factor promoting proliferation of many types of cells.[13] Systemic infusion of *HGF* has been highlighted to have potential therapeutic properties to relieve bone loss in the early phase of ovariectomy (OVX)-induced osteoporosis.[14] The increased expression of phosphatase and tensin homolog deleted on chromosome 10 (*PTEN*; known as a dual lipid and protein phosphatase) induced by inhibition of *miR-221* or *miR-26b* can be counteracted following *HGF* treatment in MSCs.[15] Knockdown of *PTEN* results in promoted bone formation and ameliorates alcohol-induced osteopenia in a mouse model.[16] Diminished *PTEN* expression is accompanied by activation of the *Wnt*/β-catenin pathway in gastric cancer cells.[17] The *Wnt*/β-catenin pathway has crucial capacity in orchestrating osteogenic differentiation of BMSCs, bone formation, and bone metabolism disorders.[18] The *Wnt*/β-catenin pathway activation could accelerate the osteogenic differentiation in human BMSCs.[19] Based on the aforementioned information, we postulated that melatonin may induce the osteogenic differentiation of BMSCs and depress OVX-induced bone loss in the pathogenesis of osteoporosis involving the regulation of *HGF*/*PTEN*/*Wnt*/β-catenin axis. To address this hypothesis, we implemented both *in vitro* and *in vivo* experiments to investigate the mechanism by which the melatonin/*HGF*/*PTEN*/*Wnt*/β-catenin axis participates in osteoporosis, shedding light on the development of a novel therapeutic strategy to prevent osteoporosis.

Materials and methods

Ethics statement
The current study was implemented under the ratification from the ethics committee of The Second Hospital of Jilin University (approval number 201908013) following the Guide for the Care and Use of Laboratory Animals published by the US National Institutes of Health. Extensive efforts were made to minimize the suffering of the included animals.

Establishment of OVX-induced osteoporosis mouse model
A total of 95 female C57BL/6 mice (aged 8-weeks old) purchased from Animal Center of Suzhou University (Jiangsu, China) were used in the study. These mice were housed under specific pathogen-free conditions (22–24°C, 50–60% humidity and a 12 h light/dark cycle) with *ad libitum* access to water and food. After 2 weeks of adaptation, the mice were treated with sham operation ($n = 20$) and OVX ($n = 75$). During the OVX operation, the mice were anesthetized with pentobarbital sodium (Sigma-Aldrich, St. Louis, USA) for 1 h (0.3 g/kg body weight in the peritoneum, Shanghai Yuanye Biotechnology Co., Ltd., Shanghai, China). The dorsal midline of the rat was curetted, and the incision was about 2 cm. After the incision was pulled to the left, a small incision of about 10 mm was cut through the abdominal wall. The ovary was exposed, and a silk knot was attached between the end of the uterine horn and the ovarian artery. After the ovaries were excised, the abdominal wall was sutured with absorbable suture, and the skin was pulled to the other side. The ovaries on the other

side were removed in the same way. After the operation, the wound was sutured, and mice were intramuscularly injected with penicillin for 3 consecutive days (80,000 units/mouse). The same procedure was performed on mice (aged 10 weeks and weighing 220–230 g), excluding ligation and ovariectomy, for sham operation. At 3 months after OVX operation, the mice were euthanized, after which the blood samples were collected, and their longitudinal bones were dissected for subsequent experiments. Seventy mice were successfully modeled, and the success rate was 92.31%.

OVX-induced osteoporosis mouse treatment

Seventy OVX mice were further grouped into OVX ($n = 20$), melatonin (Met)-1 μmol/l, Met-10 μmol/l, Met-100 μmol/l, Met-100 μmol/l + small interfering ribonucleic acid (RNA)-negative control (si-NC), and Met-100 μmol/l + si-*HGF* groups. Melatonin was dissolved in double-distilled H2O (ddH$_2$O) to prepare melatonin solution at concentration of 1 mmol/l, 10 mmol/l, and 100 mmol/l. At 1 week after the operation, the mice undergoing OVX were injected with melatonin solution *via* tail vein at a dose of 10 mg/kg twice a week for 3 months. The sham-operated mice without melatonin treatment and the mice in the OVX group were injected with the same amount of normal saline *via* tail vein. The lentiviral transfection complex was diluted in the light of the protocols of the *in vivo* transfection reagent (En-transter^{TM} *in vivo*), and the lentiviral infection was performed by tail vein injection. Each group of mice was protectively injected with a 3 μl phosphate-buffered saline mixture containing 0.5 nmol/l transfectant, strictly following manufacturer instructions, with approximately 100 μl viruses per mouse. The sham-operated mice without melatonin treatment and the mice in the OVX group were injected with the same amount of phosphate-buffered saline. The injection continuously lasted for 3 days. All oligonucleotides and plasmids were synthesized by Genechem (Shanghai, China). At 1 day before euthanasia, mice were placed in metabolic cages, followed by attaining of 24h urine. Blood was harvested from the right ventricle before euthanasia, and serum was separated for biochemical analysis. Long bones were dissected after euthanasia, placed in 0.01% sodium azide saline, and stored in a refrigerator at 4°C for histological and micro-computed tomography (micro-CT) analysis and three-dimensional (3D) reconstruction.

Biochemical measurements

Serum bone-specific alkaline phosphatase (BALP) activity was determined on the biochromatic analyzer using lectin precipitation procedure that also quantified total alkaline phosphatase (ALP) activity (tALP, Abbott VP Biochromatric Analyser, Abbott Laboratories Diagnostic Division, USA). The calcium (Ca; CA 590 Calcium kit, Randox Laboratory Ltd., UK) and phosphorus (P; PH 1016 Inorganic phosphorus kit, Randox Laboratory Ltd., UK) concentrations were evaluated in serum and urine samples with colorimetric methods. Urinary excretion of deoxypridinoline (Dpd) was assessed by immunoassay method (8007 Pyrilinks-D kit, Metra Biosystems Inc., USA). Duplicate assays were implemented for serum BALP and Ca, and urinary Ca and P, whereas a single assay was carried out for urinary Dpd.

BMSC isolation and culture

Three months after OVX, the mice were euthanized by intraperitoneal injection of pentobarbital sodium (Sigma-Aldrich) under anesthesia. Bone marrow cells were isolated from the femur by washing with α-minimum essential medium (α-MEM; M0894, Sigma-Aldrich), and the red blood cells were removed with red blood cell lysis buffer (R7757, Sigma-Aldrich). After washing, the cells were plated in standard growth medium [α-MEM supplemented with 10% fetal bovine serum (FBS), 100 U/ml penicillin and 100 μg/ml streptomycin] at 37°C. The mouse primary BMSCs were then detached with 0.25% trypsin-ethylenediaminetetraacetic acid (EDTA), and then re-plated.

BMSC treatment

As per the directions of the Lipofectamine 2000 reagents (11668-019, Invitrogen, NY, CA, USA), BMSCs were arranged into Met-1 μmol/l (BMSCs cultured in standard growth medium + 1 mmol/l melatonin), Met-10 μmol/l (BMSCs cultured in standard growth medium + 10 mmol/l melatonin), Met-100 μmol/l (BMSCs cultured in standard growth medium + 100 mmol/l melatonin), Met-100 μmol/l + small interfering RNA (si)-*HGF* (BMSCs transfected with si-*HGF* plasmid and then cultured in standard growth medium + 100 mmol/l melatonin), Met-100 μmol/l + overexpression (oe)-*PTEN* (BMSCs transfected with oe-*PTEN* plasmid and then cultured in standard growth medium + 100 mmol/l melatonin), si-*PTEN*

(BMSCs cultured in standard growth medium after transfection with si-*PTEN* plasmid), and Met-100 µmol/l + oe-DKK1 (BMSCs transfected with oe-DKK1 plasmid and then cultured in standard growth medium + 100 mmol/l melatonin) groups, as well as their controls, including control (BMSCs cultured in standard growth medium without other components), control + oe-NC [BMSCs transfected with negative control overexpression (oe-NC) plasmid and then cultured in standard growth medium], Met-100 µmol/l + si-NC (BMSCs transfected with si-NC plasmid and then cultured in standard growth medium + 100 mmol/l melatonin), control + si-NC (BMSCs transfected with si-NC plasmid and then cultured in standard growth medium), Met-100 µmol/l + oe-NC (BMSCs transfected with oe-NC plasmid and then cultured in standard growth medium + 100 mmol/l melatonin) and si-NC (BMSCs transfected with si-NC plasmid and then cultured in standard growth medium) groups. The expression plasmid vectors pcDNA3.1, the overexpression plasmid GV141, and the silencing plasmid GV248 (final concentration of 50 nmol/l and transfection amount of 500 ng) were purchased from Genechem. After 48 h, the cells were used for the subsequent experiments.

Osteogenic differentiation induction

BMSCs were cultured in 12-well plates at a density of 1×10^4 cells/cm^2. Upon reaching 80% confluence, the cells were cultured in osteogenic medium containing 10% FBS, 10 mmol/l β-glycerophosphate, 100 nmol/l dexamethasone, and 50 µg/ml dulbecco's modified Eagle's medium [DMEM] ascorbic acid) for induction, lasting for 14 days.

Cell-counting kit-8 (CCK-8) assay

With the medium discarded, 150 µl freshly prepared α-MEM containing 10% cell-counting kit (CCK)-8 solution (96992, Sigma-Aldrich) was added to each well of 96-well plates. Meanwhile, a blank control well was set, in which only a mixture of α-MEM and CCK-8 was added. The plate was then incubated at 37°C for 2 h, and the optical density value was measured at a wavelength of 450 nm on the first, third, fifth, and seventh day, respectively.

Alizarin red S (ARS) staining

At the 14th day of osteogenesis induction, the calcium deposition of BMSCs was evaluated by ARS staining. In short, BMSCs were fixed with 4% paraformaldehyde at room temperature for 30 min and incubated with 1 ml of ARS staining solution (Cyagen, USA) for 30 min at room temperature. ARS staining solution was chelated with cell calcium to form alizarin red-calcium complex, showing bright red color. The images were then captured under an Olympus IX51 microscope. For quantitative analysis, 5% perchloric acid solution was added to each well to dissolve the stains on the calcified layer. A spectrophotometer was used to measure the absorbance at 420 nm to quantify the degree of mineralization.

ALP activity and staining

At the 14th day of osteogenesis induction, BMSCs were fixed in 4% paraformaldehyde for 20 min and washed three times with distilled water. Next, the cells were stained with 5-bromo-4-chloro-3-indolyl phosphate (BCIP)/nitro blue tetrazolium (NBT) ALP Detection kit (Shanghai Beyotime Biotechnology Co. Ltd., Shanghai, China). To determine the activity of ALP, the cells on 96-well plates were lysed using lysis buffer (20 mmol/l Tris-HCl, pH 7.5, 150 mmol/l NaCl and 1% Triton X-100), followed by the addition of substrate and p-nitrophenol. ALP activity was then quantified by determining the absorbance at a wavelength of 650 nm.

Micro-computed tomography (CT) analysis of bone microstructure

The microstructural characteristics of the distal femur were examined using the Skyscan 1176 Micro-CT imaging system (Skyscan 1176, Kontich, Belgium). Bones were scanned at high resolution (18 µm) at 65 kV and 385 µA energy. A 3D reconstruction was performed using the NRecon v1.6 and CTAn v1.13.8.1 software. Region of interest was defined as the cancellous bone of the distal femur. The microstructure of bone was evaluated by calculating six parameters including BMD (mg/cm^3), bone volume/tissue volume ratio (BV/TV, %), bone surface/bone volume (BS/BV, µm^{-1}), trabecular separation (Tb. Sp, µm), trabecular thickness (Tb.Th, µm), and trabecular number (Tb.N, µm^{-1}) of distal femur cancellous. Micro-CT was analyzed back-to-back by two veterinary pathologists experienced in rodent skeletal analysis who were blinded to group allocation, and the analysis results were summarized for statistics.

Hematoxylin-eosin (HE) staining

Bone was fixed overnight in 4% paraformaldehyde and decalcified in 10% (wt/wt) EDTA (pH 7.4) for 6 weeks. Then the bone specimen was dehydrated in gradient alcohol solution, embedded in paraffin, and cut into 5 μm-thick sections. The sections were then subjected to HE staining to observe the bone structure of the distal femur. Images were finally captured under a microscope (Zeiss Axiovert 200, Obercochen, Germany).

TOPflash/FOPflash luciferase reporter assay

BMSCs were transfected with TOPflash/FOPflash luciferase reporter plasmids (12457, Addgene, Cambridge, MA, USA) to determine β-catenin/transcription factor (TCF) transcription activity. BMSCs were inoculated in 24-well plates at a density of 2×10^4 cells/well and cultured for 12 h. According to the manufacturer's instructions, TOPflash (containing repeated sequences with three TCF binding sites) or FOPflash plasmids (containing repeated sequences with three mutated TCF binding sites) were transfected into the cells. After transfection for 48 h, the luciferase activity was measured by the luciferase assay system, with the renilla luciferase activity as internal control.

Enzyme-linked immunosorbent assay (ELISA)

Mice were fasted for 4 h and then the blood samples were collected by puncturing the cheek bag. Next, the enzyme-linked immunosorbent assay (ELISA) kit was adopted to measure the serum levels of bone formation marker serum BALP (ab83369, Abcam Inc., Cambridge, UK) and bone absorption marker tartrate-resistant acid phosphatase 5b (TRAP5b; RJ15907, Renjie Biology, Shanghai, China).

Immunofluorescence staining

BMSCs were fixed with 4% paraformaldehyde for 30 min, sealed with 0.3% Triton X-100 and 1% bovine serum albumin for 30 min, and washed. Next, the cells were incubated with antibody against β-catenin (1:1600; Cell signaling technology, USA) and fluorescence-conjugated secondary antibody (Shanghai Beyotime Biotechnology Co. Ltd., Shanghai, China) for 60 min. Subsequently, the cells were treated with 4′,6-diamidino-2-phenylindole and GFP (Keygen Biotech, Nanjing, China) for 5 min to stain the nucleus. The samples were finally visualized by a confocal laser scanning microscope (Leica, Wetzlar, Germany).

Western blot analysis

Total protein was extracted from tissues and cells with the mixture of radioimmunoprecipitation assay lysis buffer (1% Triton X-100, 10 mmol/l Tris, 1 mmol/l EDTA, 1 mmol/l ethylene glycol bis [β-aminoethyl ether]-N,N'-tetraacetic acid [EGTA], and 150 mmol/l NaCl) and protease inhibitor at a ratio of 1:100. Next, protein concentration was determined by a BioRad Bradford assay kit. After separation using sodium dodecyl sulfate-polyacrylamide gel electrophoresis (SDS-PAGE), the protein was transferred onto polyvinylidene fluoride membranes. The membrane was blocked with TBST (25 mmol/l Tris, pH 7.5, 150 mmol/l NaCl and 0.1% Tween 20) with 5% bovine serum albumin, and then probed at 4°C overnight with the following primary rabbit antibodies purchased from Abcam Inc.: HGF (ab83760, 1:1000), BMP4 (ab39973, 1:1000), Runx2 (ab192256, 1:1000), Sp7 (ab22552, 1:1000), OCN (ab13418, 1:1000), OPN (ab8448, 1:1000), BMP2 (ab14933, 1:1000), PTEN (ab32199, 1:1000), β-catenin (ab32572, 1:1000), and glyceraldehyde 3-phosphate dehydrogenase (GAPDH; ab205719, 1:1000). The following day, the membrane was re-probed with horseradish peroxidase-labeled secondary antibody to goat anti-rabbit immunoglobulin G (IgG; ab205718, 1:20,000, Abcam Inc.) for 1 h. The immunocomplexes on the membrane were visualized using enhanced chemiluminescence (ECL) reagent (Thermo Fisher Scientific, Rockford, IL, USA). Chemi-Scope Mini Imaging System (Clinx Science) was used for photography. The band intensities were quantified using the ImageJ software (National Institutes of Health, Bethesda, Maryland, USA). Relative protein expression = gray value of target protein/gray value of GAPDH protein.[20]

Immunohistochemistry

The tissues were cut into 4 μm-thick sections, followed by dewaxing and dehydration. Then the tissue sections were immunostained with the following diluted antibodies purchased from Abcam Inc.: rabbit monoclonal antibody to PTEN (ab32199, 1:1000), rabbit polyclonal antibody to Wnt (ab15251, 1:1000), and rabbit monoclonal antibody to β-catenin (ab32572, 1:1000). Next, the tissue sections were incubated with biotin-labeled

secondary goat anti-rabbit IgG (ab6721, 1:1000, Abcam Inc.) for 30 min. After staining with 3,3′-diaminobenzidine (DAB; DA1010, Beijing Solarbio Science and Technology Co. Ltd., Beijing, China), the sections were dehydrated, cleared, and mounted. Finally, five high-power visual fields were randomly selected from each section and 100 cells were counted in each field under a light microscope (XSP-36, Boshida Optical Instrument Co. Ltd., Shenzhen, China). Positive cells < 5% are negative, and positive cells ≥ 5% are positive. The results were scored by two people independently.

RNA isolation and quantitation

Total RNA content was extracted from tissues using TRIzol reagents (15596026, Invitrogen). The extracted RNA was reverse transcribed into complementary deoxyribonucleic acid (cDNA) using PrimerScript RT reagent Kit (Takara, Shiga, Japan) and SYBR Premix EX Taq Kit (RR420A, Takara). Real-time qualitative polymerase chain reaction (RT-qPCR) was conducted on an ABI 7500 instrument (Applied Biosystems, Foster City, CA, USA). All investigations involved at least three wells, each repeated in triplicate. With β-actin gene as the internal reference, the fold changes were calculated using relative quantification (the $2^{-\triangle\triangle Ct}$ method). The primers are shown in Table 1.

Statistical analysis

Statistical analyses were performed using the SPSS 21.0 software (IBM Corp. Armonk, NY, USA). Measurement data were expressed as mean ± standard deviation. Data between two groups were compared using unpaired t test. Data among multiple groups were compared by one-way analysis of variance (ANOVA) with Tukey's test while data at different time points were analyzed by two-way ANOVA with Bonferroni's correction. A value of $p < 0.05$ was indicative of statistical significance.

Results

Melatonin prevents bone loss in OVX mice

OVX mice showed obvious bone loss when compared to the sham-operated mice, while treatment of melatonin improved bone mass growth [Figure 1(b)]. Bone demineralization markers in each group were detected by biochemical analysis. As shown in Supplementary Table 1 or Figure 1(a), urinary Dpd, urinary calcium excretion, serum Ca, serum P, and BALP were significantly increased in OVX mice compared with sham-operated mice ($p < 0.01$). After melatonin treatment, urinary Dpd, urinary calcium excretion, serum Ca, serum P, and BALP were reduced in a dose-dependent manner ($p < 0.01$). In addition, a decline was found in the BMD, ratio of BV/TV, Tb.Th, and Tb.N, while BS/BV and Tb.Sp were increased in OVX mice ($p < 0.01$). However, treatment with melatonin enhanced the BMD, ratio of BV/TV, Tb.Th and Tb.N but decreased BS/BV ratio and Tb.Sp in a dose-dependent manner [$p < 0.01$; Figure 1(c)–(h)]. The quantitative analysis of the trabecular microstructure of the femur further verified the above results, indicating that melatonin could reduce the bone loss of OVX mice. Furthermore, ELISA detected downregulated BALP serum levels and increased TRAP5b serum levels in OVX mice relative to sham-operated mice ($p < 0.01$). Melatonin treatment resulted in dose-dependent increase in BALP serum levels while TRAP5b serum levels were decreased in a dose-dependent manner [$p < 0.01$; Figure 1(i) and (j)]. These results suggested that melatonin had the potential to mitigate the bone loss in OVX mice.

Melatonin accelerates the osteogenic differentiation of BMSCs in vitro

We then proceeded to examine the mechanism by which melatonin inhibits bone loss. After separation from mice, BMSCs in OVX mice showed similar cell morphologic characteristics to those of sham-operated mice [Figure 2(a)]. As shown in Figure 2(b), the proliferation of BMSCs was potentiated upon melatonin treatment, showing a dose-dependent manner ($p < 0.01$). The results of ARS and ALP [Figure 2(c) and (d)] revealed an increase in the stained area and density of mineralization and calcification of BMSCs following melatonin treatment in a dose-dependent manner ($p < 0.01$), indicating that melatonin might promote the differentiation of BMSCs into osteoblasts. Additionally, the expression of osteogenic-related factors was detected in BMSCs by Western blot analysis. As shown in Figure 2(e), the protein expression of BMP4, Runx2, Sp7, OCN, OPN and BMP2 was higher in BMSCs treated with melatonin than those in the control cells ($p < 0.01$), with a dose-dependent increase ($p < 0.01$). These data indicated that

Table 1. Primer sequences for RT-qPCR.

Gene	Sequences (5′–3′)
HGF	F: AAACATATCTGCGGAGGATC
	R: ACGATTTGGAATGGCACATC
PTEN	F: TGGATTCGACTTAGACTTGACCT
	R: TGCTTTGAATCCAAAAACCTTACT
Oct4	F: GAGGAGTCCCAGGACATGAA
	R: AGATGGTGGTCTGGCTGAAC
Cyclin D1	F: TCAAGTGTGACCCGGACTG
	R: CTCCAGAAGGGCTTCAATCTGT
C-myc	F: CGAGGAGAATGTCAAGAGGCGAAC
	R: GCTTGGACGGACAGGATGTATGC
CD44	F: TCAGAGGAGTAGGAGAGAGGAAAC
	R: GAAAAGTCAAAGTAACAATAACAGTGG
GAPDH	F: CATGAGAAGTATGACAACAGCCT
	R: AGTCCTTCCACGATACCAAAGT

GADPH, glyceraldehyde 3-phosphate dehydrogenase; RT-qPCR, real-time qualitative polymerase chain reaction.

melatonin could promote osteogenic differentiation of BMSCs *in vitro*.

Melatonin promotes the differentiation of BMSCs into osteoblasts by upregulating transcription factor HGF in BMSCs

Next, we aimed to exploit the possible relationship between melatonin and transcription factor *HGF*. The results of RT-qPCR and Western blot analysis revealed that *HGF* expression was downregulated in the femur of OVX mice ($p < 0.01$), which was upregulated upon melatonin treatment in a dose-dependent manner [$p < 0.01$; Figure 3(a) and (b)]. The finding suggested the ability of melatonin to upregulate *HGF* in mice. Next, we intended to verify the regulatory effect of melatonin on *HGF* expression *in vitro*. As shown in Figure 3(c) and (d), melatonin treatment resulted in elevation in *HGF* expression in a dose-dependent manner ($p < 0.01$), which was consistent with the results observed *in vivo*. Therefore, melatonin elevated *HGF* expression both *in vivo* and *in vitro*.

Subsequently, we performed a series of *in vitro* experiments to explore whether melatonin can promote the differentiation of BMSCs into osteoblasts by regulating transcription factor *HGF*. The silencing efficiency of *HGF* was confirmed by RT-qPCR, manifested by reduced expression of *HGF* in BMSCs treated with si-*HGF*-1 or si-*HGF*-2, of which si-*HGF*-2 showed a superior silencing efficiency ($p < 0.01$), and was thus selected for the following experiments [Figure 3(e)]. Moreover, *HGF* expression was elevated in Met-100 µmol/l-treated BMSCs ($p < 0.01$) while it was diminished in BMSCs treated with Met-100 µmol/l + si-*HGF* [$p < 0.01$; Figure 3(f) and (g)]. This indicated that knockdown of *HGF* reversed the upregulation of melatonin on *HGF* expression. The results of CCK-8 assay demonstrated that Met-100 µmol/l increased the proliferation of BMSCs while treatment with Met-100 µmol/l + si-*HGF* led to opposite results [$p < 0.01$; Figure 3(h)], which revealed that knockdown of *HGF* could reverse the promoting effect of melatonin on the proliferation of BMSCs. Figure 3(i) and (j) clarified that the mineralization and calcification of BMSCs were enhanced in response to Met-100 µmol/l treatment ($p < 0.01$), which was negated by treatment with Met-100 µmol/l + si-*HGF* ($p < 0.01$), indicating that knockdown *HGF* inhibited the osteogenic differentiation of BMSCs. Besides, the protein levels of BMP4, Runx2, Sp7, OCN, OPN and BMP2 were observed to be increased following Met-100 µmol/l treatment ($p < 0.01$), while treatment with Met-100 µmol/l + si-*HGF* counteracted the results [$p < 0.01$; Figure 3(k)]. These results suggested that melatonin promoted the differentiation of BMSCs into osteoblasts by upregulating *HGF in vitro*.

Melatonin regulates the differentiation of BMSCs into osteoblasts via HGF-dependent PTEN expression in BMSCs

After uncovering the regulatory role of melatonin in the *HGF* expression, we next aimed to investigate the possible downstream mechanism of the *HGF* transcription factor. As illustrated in Figure 4(a) and (b), *PTEN* expression was augmented in OVX mice ($p < 0.01$). Besides, *HGF* expression was found to be upregulated while *PTEN* expression was downregulated in BMSCs following Met-100 µmol/l treatment ($p < 0.01$), which was neutralized upon treatment with

(a)

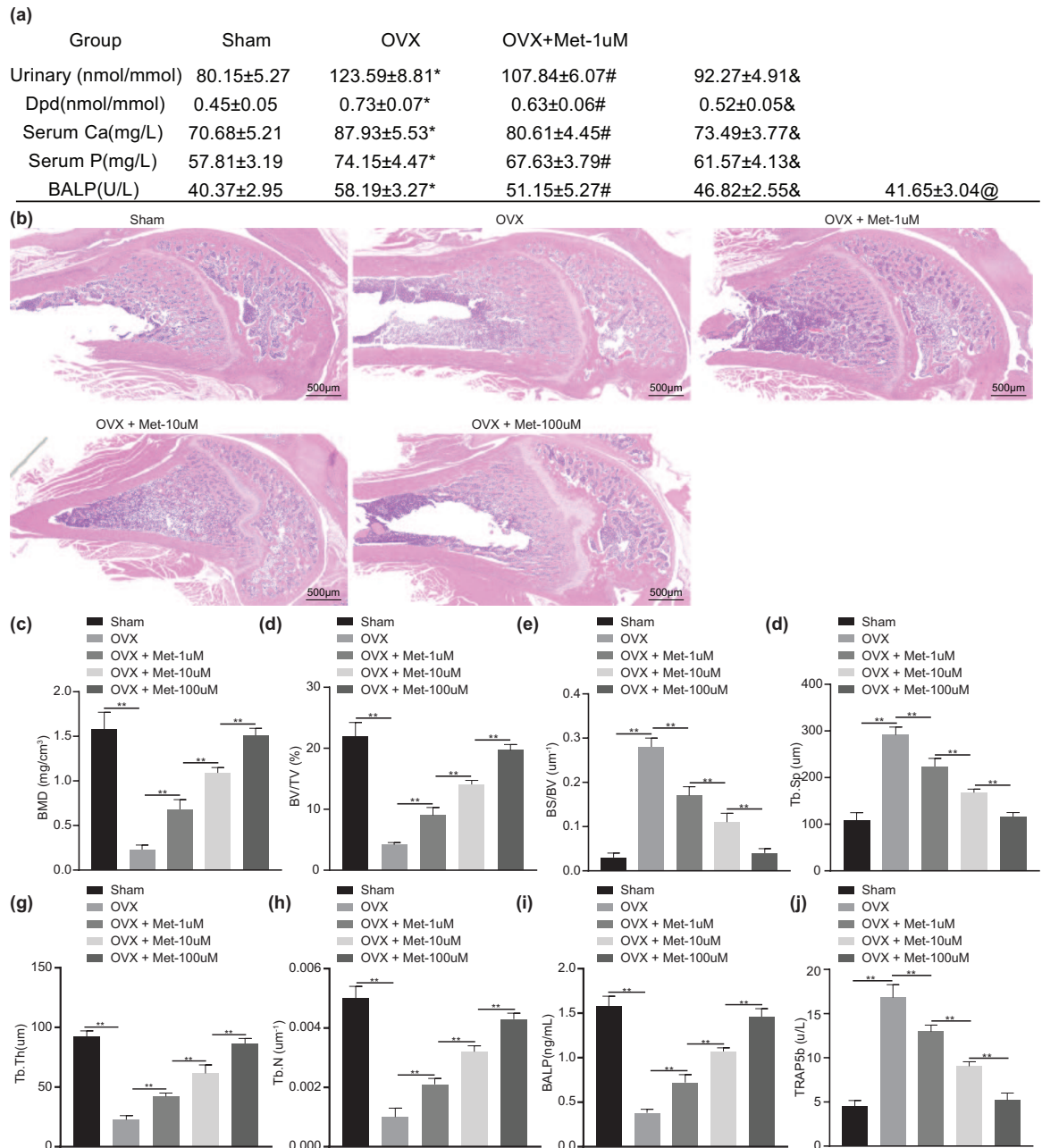| Group	Sham	OVX	OVX+Met-1uM		
Urinary (nmol/mmol)	80.15±5.27	123.59±8.81*	107.84±6.07#	92.27±4.91&	
Dpd(nmol/mmol)	0.45±0.05	0.73±0.07*	0.63±0.06#	0.52±0.05&	
Serum Ca(mg/L)	70.68±5.21	87.93±5.53*	80.61±4.45#	73.49±3.77&	
Serum P(mg/L)	57.81±3.19	74.15±4.47*	67.63±3.79#	61.57±4.13&	
BALP(U/L)	40.37±2.95	58.19±3.27*	51.15±5.27#	46.82±2.55&	41.65±3.04@

Figure 1. Melatonin attenuates the bone loss in OVX mice.
OVX mice were treated with melatonin at different concentrations. (a) Bone demineralization markers in serum and urine as detected by biochemical analysis. (b) HE staining analysis in the bone structure of mouse distal femur (scale bar = 500 μm). (c) Micro-CT quantitative analysis of BMD in mouse femur. (d) Micro-CT quantitative analysis of BV/TV ratio in mouse femur. (e) Micro-CT quantitative analysis of BS/BV ratio in mouse femur. (f) Micro-CT quantitative analysis of Tb.Sp in mouse femur. (g) Micro-CT quantitative analysis of Tb.Th in mouse femur. (h) Micro-CT quantitative analysis of Tb.N in mouse femur. (i) Serum levels of BALP measured by ELISA. (j) Serum levels of TRAP5b measured by ELISA.
**$p < 0.01$, indicates statistical significance. Data (mean ± standard deviation) among multiple groups were compared by one-way ANOVA with Tukey's test. $n = 10$ for mice following each treatment.
ANOVA, analysis of variance; BALP, bone-specific alkaline phosphatase; BS, bone surface; BV, bone volume; Ca, calcium; CT, computed tomography; Dpd, deoxypridinoline; ELISA, enzyme-linked immunosorbent assay; HE, hematoxylin eosin; Met, melatonin; P, phosphorus; Tb.N, trabecular number; Tb.Sp, trabecular separation; Tb.Th, trabecular thickness.
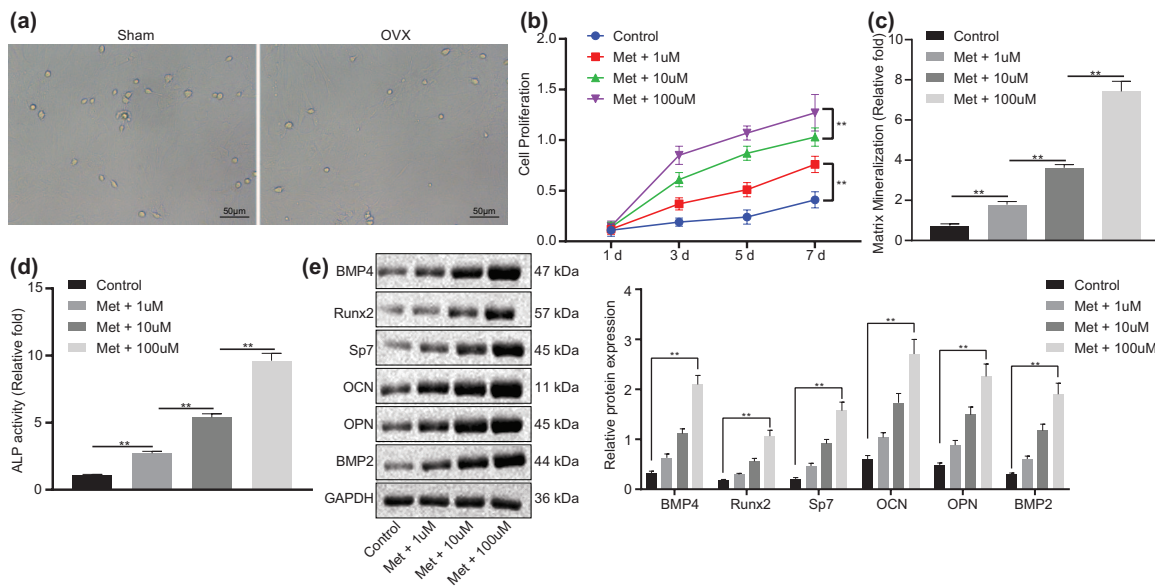
Figure 2. Melatonin augments osteogenic differentiation of BMSCs *in vitro*.
(a) Morphologic characteristics of the isolated BMSCs from the OVX and sham-operated mice observed by optical microscope (scale bar = 50 μm). (b) Proliferation of BMSCs treated with melatonin at different concentrations measured by CCK-8 assay. (c) Mineralization of BMSCs treated with melatonin at different concentrations evaluated by ARS staining. (d) Calcification of BMSCs treated with melatonin at different concentrations evaluated by ALP activity and staining. (e) Western blot analysis of BMP4, Runx2, Sp7, OCN, OPN and BMP2 protein expression in BMSCs treated with melatonin at different concentrations.
$^{**}p < 0.01$, indicates statistical significance. Data (mean ± standard deviation) among multiple groups were compared by one-way ANOVA with Tukey's test while those at different time points were compared by two-way ANOVA with Bonferroni's correction. Cell experiments were conducted in triplicate.
ALP, alkaline phosphatase; ANOVA, analysis of variance; ARS, alizarin red S; BMSCs, bone marrow mesenchymal stem cells; CCK, cell-counting kit; GAPDH, glyceraldehyde 3-phosphate dehydrogenase; Met, melatonin; OVX, ovariectomy.

Met-100 μmol/l + si-*HGF* [$p < 0.01$; Figure 4(c) and (d)], which implied that knockdown of *HGF* reversed the inhibition of melatonin on *PTEN*.

Subsequently, RT-qPCR verified the overexpression efficiency of *PTEN*, manifested by elevated *PTEN* expression in BMSCs transfected with oe-*PTEN* [$p < 0.01$; Figure 4(e)]. *HGF* expression showed an enhancement in Met-100 μmol/l-treated cells ($p < 0.01$), while that of *PTEN* presented a decline ($p < 0.01$). However, there was no significant difference in the mRNA and protein expression of *HGF* ($p > 0.01$) but that of *PTEN* was increased in cells treated with Met-100 μmol/l + oe-*PTEN* [$p < 0.01$; Figure 4(f) and (g)]. The results of CCK-8, as shown in Figure 4(h), revealed ascending cell proliferation trend in response to Met-100 μmol/l ($p < 0.01$), while it was impaired upon Met-100 μmol/l + oe-*PTEN* treatment ($p < 0.01$), indicating that *PTEN* disrupted the promoting effect of melatonin on BMSC proliferation. Moreover, there were

increased mineralization and calcification of Met-100 μmol/l-treated cells ($p < 0.01$), while Met-100 μmol/l + oe-*PTEN* treatment undermined the trend [$p < 0.01$; Figure 4(i) and (j)], indicating that *PTEN* inhibited the osteogenic differentiation of BMSCs. In addition, Figure 4(k) presents enforced protein expression of BMP4, Runx2, Sp7, OCN, OPN and BMP2 in response to Met-100 μmol/l ($p < 0.01$), while Met-100 μmol/l + oe-*PTEN* treatment led to opposite results ($p < 0.01$). Based on the results obtained, melatonin could regulate the differentiation of BMSCs into osteoblasts through the *HGF*/*PTEN* axis in BMSCs.

Knockdown of PTEN facilitates activation of the Wnt/β-catenin pathway in BMSCs

A downward inclination was observed in the protein expression of β-catenin in the femur of OVX mice [$p < 0.01$; Figure 5(a)], which was negatively correlated with *PTEN* expression and therefore, we speculated that *PTEN* might inhibit
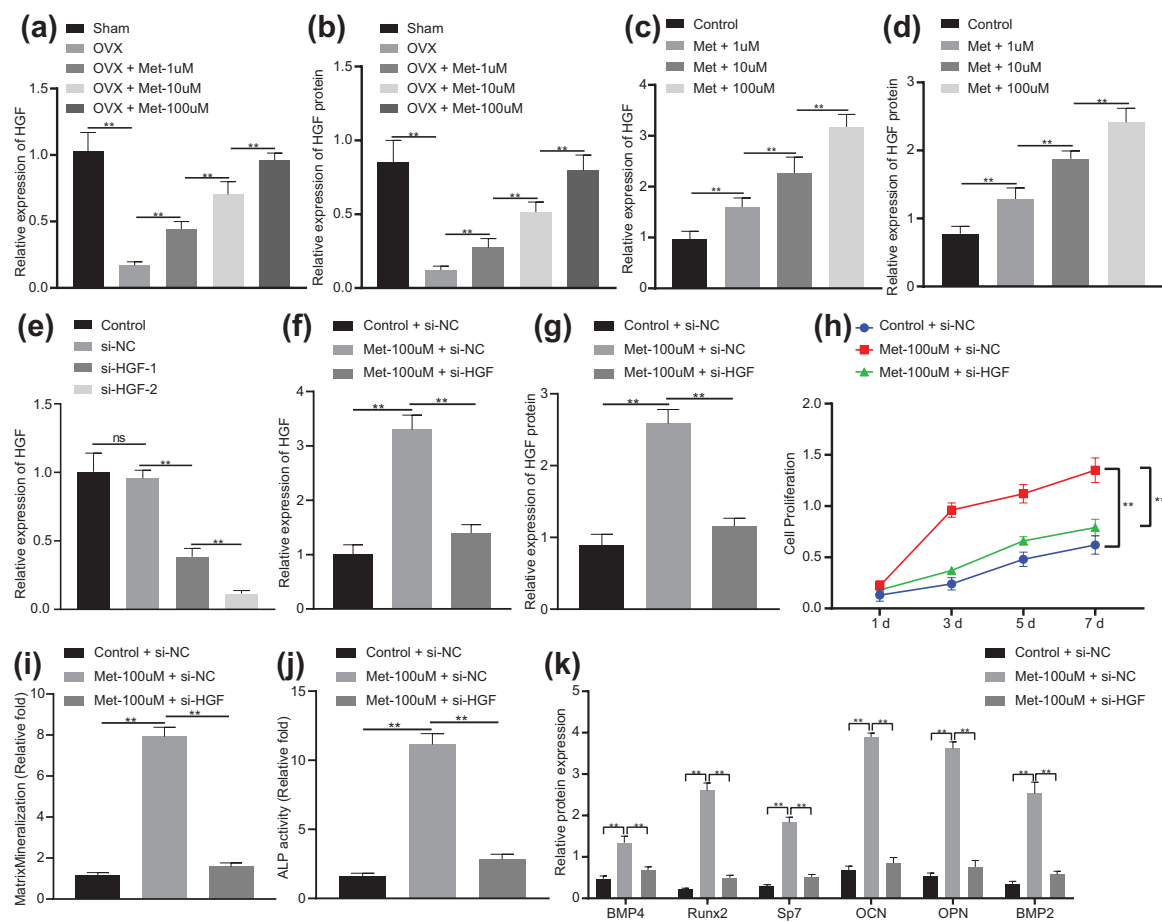
Figure 3. Melatonin facilitates the differentiation of BMSCs into osteoblasts *via HGF* upregulation in BMSCs. (a) mRNA expression of *HGF* in the femur of OVX or OVX mice treated with melatonin at different concentrations determined by RT-qPCR ($n = 10$). (b) Western blot analysis of HGF protein expression in the femur of OVX or OVX mice treated with melatonin at different concentrations ($n = 10$). (c) mRNA expression of *HGF* in BMSCs treated with melatonin at different concentrations determined by RT-qPCR. (d) Western blot analysis of HGF protein expression in BMSCs treated with melatonin at different concentrations. (e) Silencing efficiency of *HGF* in BMSCs confirmed by RT-qPCR. (f) mRNA expression of *HGF* in BMSCs treated with Met-100 µmol/l or in combination with si-*HGF* determined by RT-qPCR. (g) Western blot analysis of HGF protein expression in BMSCs treated with Met-100 µmol/l or in combination with si-*HGF*. (h) Proliferation of BMSCs treated with Met-100 µmol/l or in combination with si-*HGF* measured by CCK-8 assay. (i) Mineralization of BMSCs treated with Met-100 µmol/l or in combination with si-*HGF* evaluated by ARS staining. (j) Calcification of BMSCs treated with Met-100 µmol/l or in combination with si-*HGF* evaluated by ALP activity and staining. (k) Western blot analysis of BMP4, Runx2, Sp7, OCN, OPN and BMP2 protein expression in BMSCs treated with Met-100 µmol/l or in combination with si-*HGF*. **$p < 0.01$, indicates statistical significance. Data (mean ± standard deviation) among multiple groups were compared by one-way ANOVA with Tukey's test while those at different time points were compared by two-way ANOVA with Bonferroni's correction. Cell experiments were conducted in triplicate.

ALP, alkaline phosphatase; ANOVA, analysis of variance; ARS, alizarin red S; BMSCs, bone marrow mesenchymal stem cells; Met, melatonin; mRNA, messenger ribonucleic acid; OVX, ovariectomy; RT-qPCR, real-time qualitative polymerase chain reaction; si-, small interfering.

the *Wnt*/β-catenin pathway. To address this hypothesis, we first performed RT-qPCR and Western blot analysis to detect the silencing efficiency of *PTEN* in cells. The results displayed reduced *PTEN* expression in cells treated with si-*PTEN*-1 or si-*PTEN*-2 ($p < 0.01$), with a more pronounced decline in response to si-*PTEN*-2 [Figure 5(b) and

(c)]. si-*PTEN*-2 was thus used in subsequent experiments. As shown in Figure 5(d), the activity of TOPflash was increased in si-*PTEN*-treated cells ($p < 0.01$). In addition, β-catenin protein was upregulated in si-*PTEN*-treated cells [$p < 0.01$; Figure 5(e)]. The nuclear accumulation of β-catenin was found to be increased in cells following *PTEN* knockdown [$p < 0.01$; Figure 5(f)].
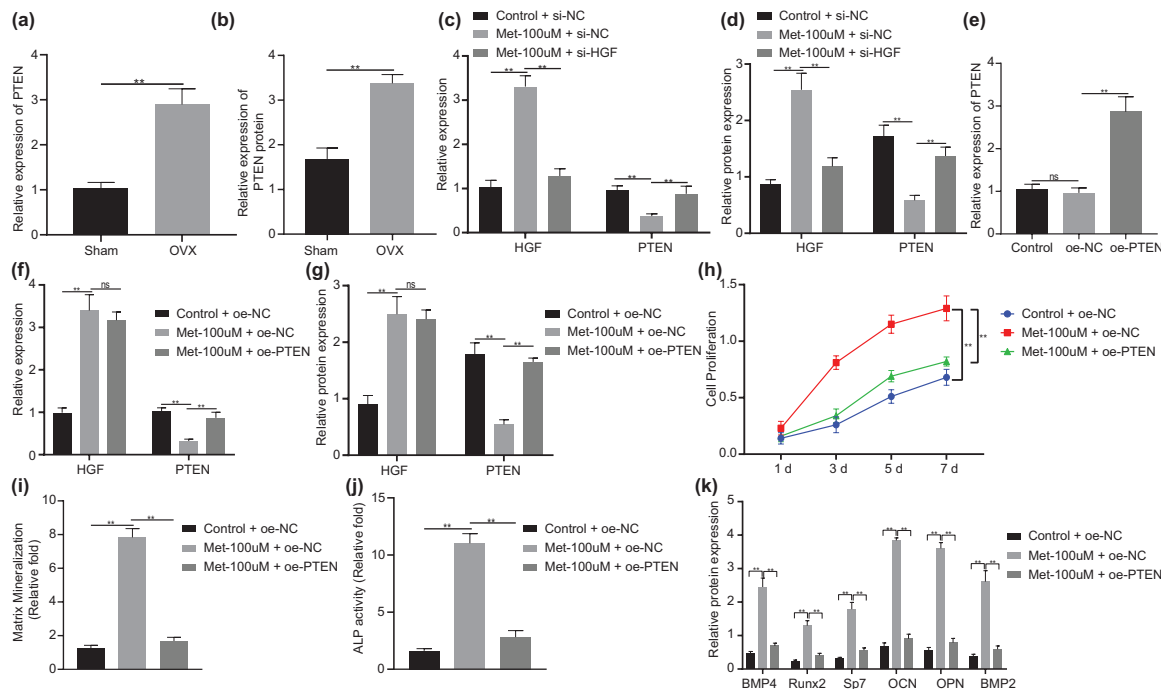
Figure 4. Melatonin affects osteogenic differentiation of BMSCs *via* the *HGF/PTEN* axis in BMSCs.
(a) mRNA expression of *PTEN* in the femur of OVX or sham-operated mice determined by RT-qPCR ($n = 10$). (b) Western blot analysis of PTEN protein expression in the femur of OVX or sham-operated mice ($n = 10$). (c) mRNA expression of *HGF* and *PTEN* in BMSCs treated with Met-100 μmol/l or in combination with si-*HGF* determined by RT-qPCR. (d) Western blot analysis of HGF and PTEN protein expression in BMSCs treated with Met-100 μmol/l or in combination with si-*HGF*. (e) Overexpression efficiency of *PTEN* in BMSCs confirmed by RT-qPCR. (f) mRNA expression of *HGF* and *PTEN* in BMSCs treated with Met-100 μmol/l or in combination with oe-*PTEN* determined by RT-qPCR. (g) Western blot analysis of HGF and PTEN protein expression in BMSCs treated with Met-100 μmol/l or in combination with oe-*PTEN*. (h) Proliferation of BMSCs treated with Met-100 μmol/l or in combination with oe-*PTEN* measured by CCK-8 assay. (i) Mineralization of BMSCs treated with Met-100 μmol/l or in combination with oe-*PTEN* evaluated by ARS staining. (j) Calcification of BMSCs treated with Met-100 μmol/l or in combination with oe-*PTEN* evaluated by ALP activity and staining. (k) Western blot analysis of BMP4, Runx2, Sp7, OCN, OPN and BMP2 protein expression in BMSCs treated with Met-100 μmol/l or in combination with oe-*PTEN*.
$**p < 0.01$, indicates statistical significance. Data (mean ± standard deviation) among multiple groups were compared by one-way ANOVA with Tukey's test while those at different time points were compared by two-way ANOVA with Bonferroni's correction. Cell experiments were conducted in triplicate.
ALP, alkaline phosphatase; ANOVA, analysis of variance; BMSCs, bone marrow mesenchymal stem cells; CCK, cell-counting kit; Met, melatonin; mRNA, messenger ribonucleic acid; oe-, overexpression; OVX, ovariectomy; RT-qPCR, real-time qualitative polymerase chain reaction.

Furthermore, *Oct4, Cyclin D1, C-myc* and *CD44* exhibited amplified expression in si-*PTEN*-treated cells [$p < 0.01$; Figure 5(g)]. The data supported that inhibition of *PTEN* could activate the *Wnt*/β-catenin pathway in BMSCs.

Melatonin elicits osteogenic differentiation of BMSCs via the HGF/PTEN/Wnt/β-catenin pathway in BMSCs

Since *PTEN* knockdown can activate the *Wnt*/β-catenin pathway in BMSCs, we aimed to explore the regulatory mechanism by which melatonin regulates the *Wnt*/β-catenin pathway through *PTEN*. As shown in Figure 6(a) to (c), an elevation was found in *HGF* expression, TOPflash activity, and β-catenin protein expression ($p < 0.01$) while *PTEN* expression was decreased in Met-100 μmol/l-treated cells ($p < 0.01$), which demonstrated that melatonin could promote the *Wnt*/β-catenin pathway. In response to Met-100 μmol/l + oe-*PTEN*, TOPflash activity and β-catenin protein expression were decreased ($p < 0.01$), while *PTEN* was upregulated in cells ($p < 0.01$), indicating that *PTEN* reversed the promoting effect of melatonin on the *Wnt*/β-catenin pathway.

Treatment with Met-100 μmol/l led to higher *HGF* expression, TOPflash activity, and β-catenin protein expression while lower *PTEN*
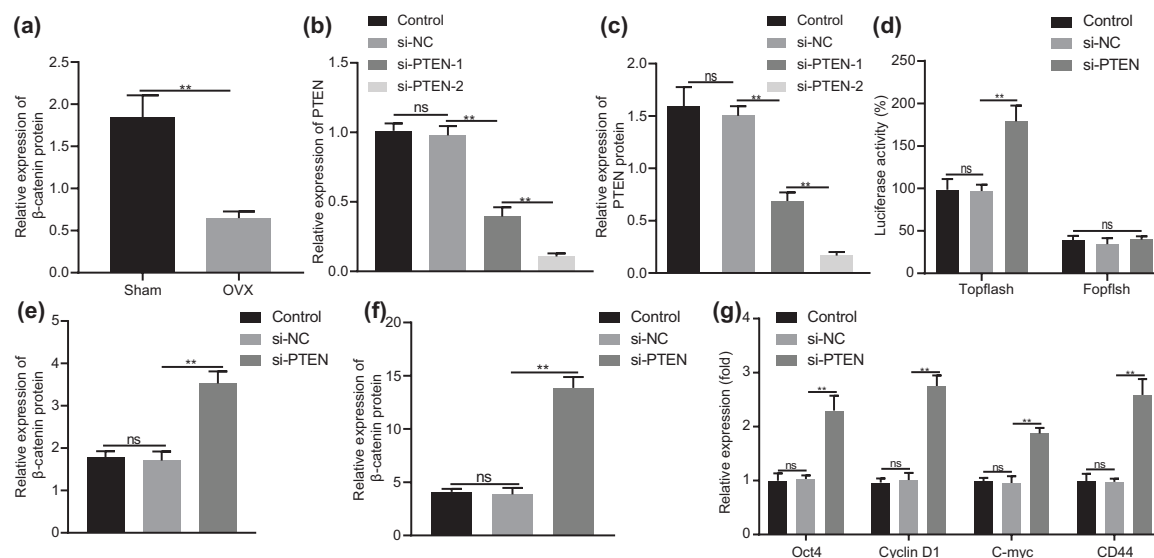
Figure 5. *PTEN* knockdown induces activation of the *Wnt*/β-catenin pathway in BMSCs.
(a) Western blot analysis of β-catenin protein expression in the femur of OVX or sham-operated mice ($n = 10$). (b) mRNA expression of *PTEN* in cells treated with si-*PTEN*-1 or si-*PTEN*-2 determined by RT-qPCR. (c) Western blot analysis of PTEN protein expression in cells treated with si-*PTEN*-1 or si-*PTEN*-2. (d) Activity of TOPflash in cells treated with si-*PTEN* detected by dual-luciferase reporter. (e) Western blot analysis of β-catenin protein expression in BMSCs treated with si-*PTEN*. (f) Nuclear accumulation of β-catenin in BMSCs treated with si-*PTEN* determined by immunofluorescence staining. (g) mRNA expression of *Oct4, Cyclin D1, C-myc* and *CD44* in BMSCs treated with si-*PTEN* determined by RT-qPCR.
$**p < 0.01$, indicates statistical significance. Data (mean ± standard deviation) between two groups were compared using unpaired *t* test while those among multiple groups were compared by one-way ANOVA with Tukey's test. Cell experiments were conducted in triplicate.
ANOVA, analysis of variance; BMSCs, bone marrow mesenchymal stem cells; mRNA, messenger ribonucleic acid; OVX, ovariectomy; RT-qPCR, real-time qualitative polymerase chain reaction; si-, small interfering.

expression in BMSCs than control BMSCs. By contrast, Met-100 μmol/l + DKK1 treatment downregulated TOPflash activity and β-catenin protein expression [$p < 0.01$; Figure 6(d)–(f)], indicating that DKK1 inhibited the activity of the *Wnt*/β-catenin pathway. In addition, the enhanced proliferation of BMSCs by Met-100 μmol/l treatment ($p < 0.01$) was reversed by DKK1 treatment [$p < 0.01$; Figure 6(g)], indicating that inhibition of *Wnt*/β-catenin pathway inhibited the proliferation of BMSCs. Furthermore, there were increased mineralization and calcification in cells treated with Met-100 μmol/l ($p < 0.01$), which was negated by DKK1 treatment [$p < 0.01$; Figure 6(h) and (i)], indicating that inhibited *Wnt*/β-catenin undermined the melatonin-induced osteogenic differentiation of BMSCs. In addition, Figure 6(j) exhibits augmented protein expression of BMP4, Runx2, Sp7, OCN, OPN, and BMP2 in response to Met-100 μmol/l ($p < 0.01$), while DKK1 treatment led to opposite results ($p < 0.01$). These results suggested that melatonin inhibited *PTEN* expression and then activated the *Wnt*/β-catenin

pathway, thus promoting osteogenic differentiation of BMSCs in BMSCs.

Melatonin ameliorates osteoporosis through the HGF/PTEN/Wnt/β-catenin axis in OVX mice

We then intended to investigate the effect of melatonin-mediated *HGF*/*PTEN*/*Wnt*/β-catenin axis on osteoporosis in OVX mice. As shown in Figure 7(a) and (b), there were higher *HGF* expression and β-catenin protein expression, while lower *PTEN* expression in Met-100 μmol/l-treated mice than OVX mice ($p < 0.01$). In response to Met-100 μmol/l + si-*HGF*, the β-catenin protein was downregulated ($p < 0.01$), while *PTEN* was upregulated ($p < 0.01$). Knockdown of *HGF* reversed the inhibition of melatonin on *PTEN* expression and the promotion on the *Wnt* and β-catenin expression [$p < 0.01$; Figure 7(c), Supplementary Figure 1(a)].

OVX mice showed obvious bone loss which was alleviated by treatment of Met-100 μmol/l. However, further treatment with si-*HGF* led to reduced bone mass

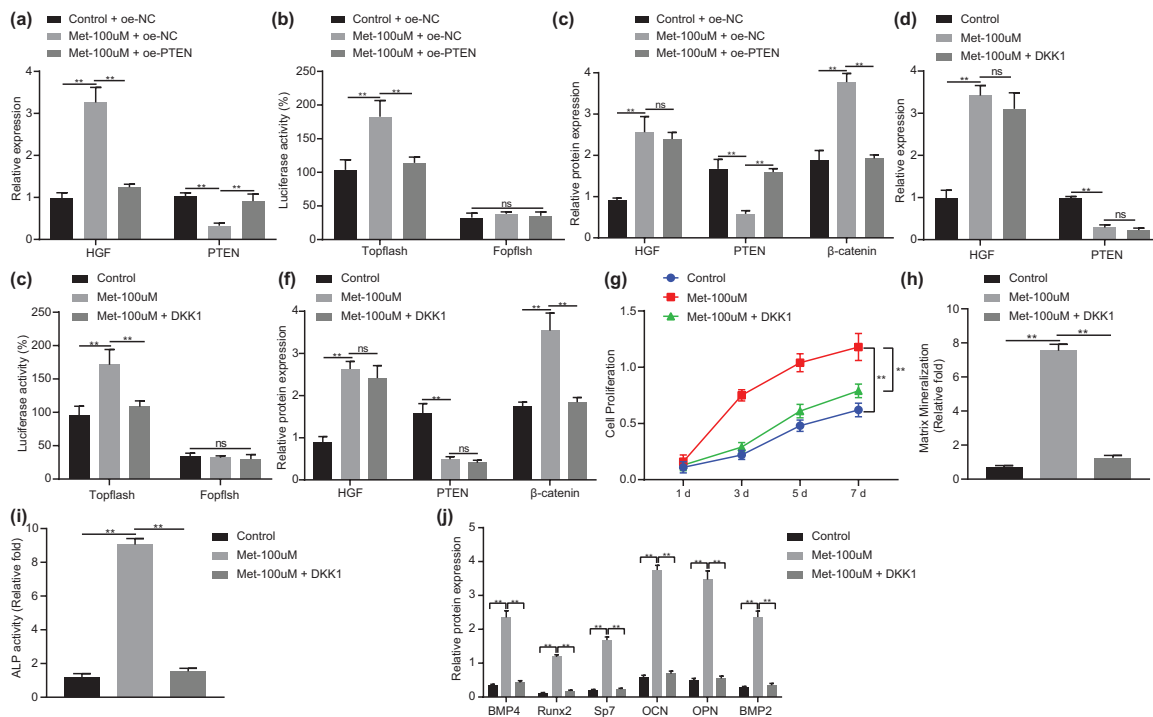**Figure 6.** Melatonin stimulates osteogenic differentiation of BMSCs *via* the *HGF*/*PTEN*/*Wnt*/β-catenin axis in BMSCs.
(a) mRNA expression of *HGF* and *PTEN* in BMSCs treated with Met-100 μmol/l or in combination with oe-*PTEN* determined by RT-qPCR. (b) Activity of TOPflash in BMSCs treated with Met-100 μmol/l or in combination with oe-*PTEN* detected by dual-luciferase reporter. (c) Western blot analysis of HGF, PTEN and β-catenin protein expression in BMSCs treated with Met-100 μmol/l or in combination with oe-*PTEN*. (d) mRNA expression of *HGF* and *PTEN* in BMSCs treated with Met-100 μmol/l or in combination with DKK1 determined by RT-qPCR. (e) Activity of TOPflash in BMSCs treated with Met-100 μmol/l or in combination with DKK1 detected by dual-luciferase reporter. (f) Western blot analysis of HGF, PTEN and β-catenin protein expression in BMSCs treated with Met-100 μmol/l or in combination with DKK1. (g) Proliferation of BMSCs treated with Met-100 μmol/l or in combination with DKK1 measured by CCK-8 assay. (h) Mineralization of BMSCs treated with Met-100 μmol/l or in combination with DKK1 evaluated by ARS staining. (i) Calcification of BMSCs treated with Met-100 μmol/l or in combination with DKK1 evaluated by ALP activity and staining. (j) Western blot analysis of BMP4, Runx2, Sp7, OCN, OPN and BMP2 protein expression in BMSCs treated with Met-100 μmol/l or in combination with DKK1. **$p < 0.01$, indicates statistical significance. Data (mean ± standard deviation) among multiple groups were compared by one-way ANOVA with Tukey's test while those at different time points were compared by two-way ANOVA with Bonferroni's correction. Cell experiments were conducted in triplicate.
ALP, alkaline phosphatase; ANOVA, analysis of variance; ARS, alizarin red S; BMSCs, bone marrow mesenchymal stem cells; CCK, cell-counting kit; Met, melatonin; mRNA, messenger ribonucleic acid; oe-, overexpression; OVX, ovariectomy; RT-qPCR, real-time qualitative polymerase chain reaction.

[Supplementary Figure 1(b)]. In addition, biochemical analysis (Supplementary Table 2), urinary Dpd, urinary calcium excretion, serum Ca, serum P, and BALP were increased in OVX mice in contrast to the sham-operated mice ($p < 0.01$). After Met-100 μmol/l treatment, urinary Dpd, urinary Ca, serum Ca, serum P, BALP in femoral bone of OVX mice were diminished ($p < 0.01$). In the presence of Met-100 μmol/l, urinary Dpd, urinary Ca, serum Ca, serum P, and BALP in OVX mice were augmented by silencing *HGF* ($p < 0.01$). A reduction was found in the BMD, ratio of BV/TV, Tb.Th, and Tb.N, while BS/BV and

Tb.Sp were increased in OVX mice ($p < 0.01$). Treatment with Met-100 μmol/l enhanced the BMD, ratio of BV/TV, Tb.Th, and Tb.N but decreased BS/BV ratio and Tb.Sp [$p < 0.01$; Figure 7(d)–(i)]. The quantitative analysis of the trabecular microstructure of the femur further verified the above results, indicating that melatonin could reduce the bone loss of OVX mice *via* mediating the *HGF*/*PTEN*/*Wnt*/β-catenin axis. Furthermore, ELISA detected downregulated BALP serum levels and increased TRAP5b serum levels in OVX mice relative to sham-operated mice ($p < 0.01$). Met-100 μmol/l treatment led to elevated
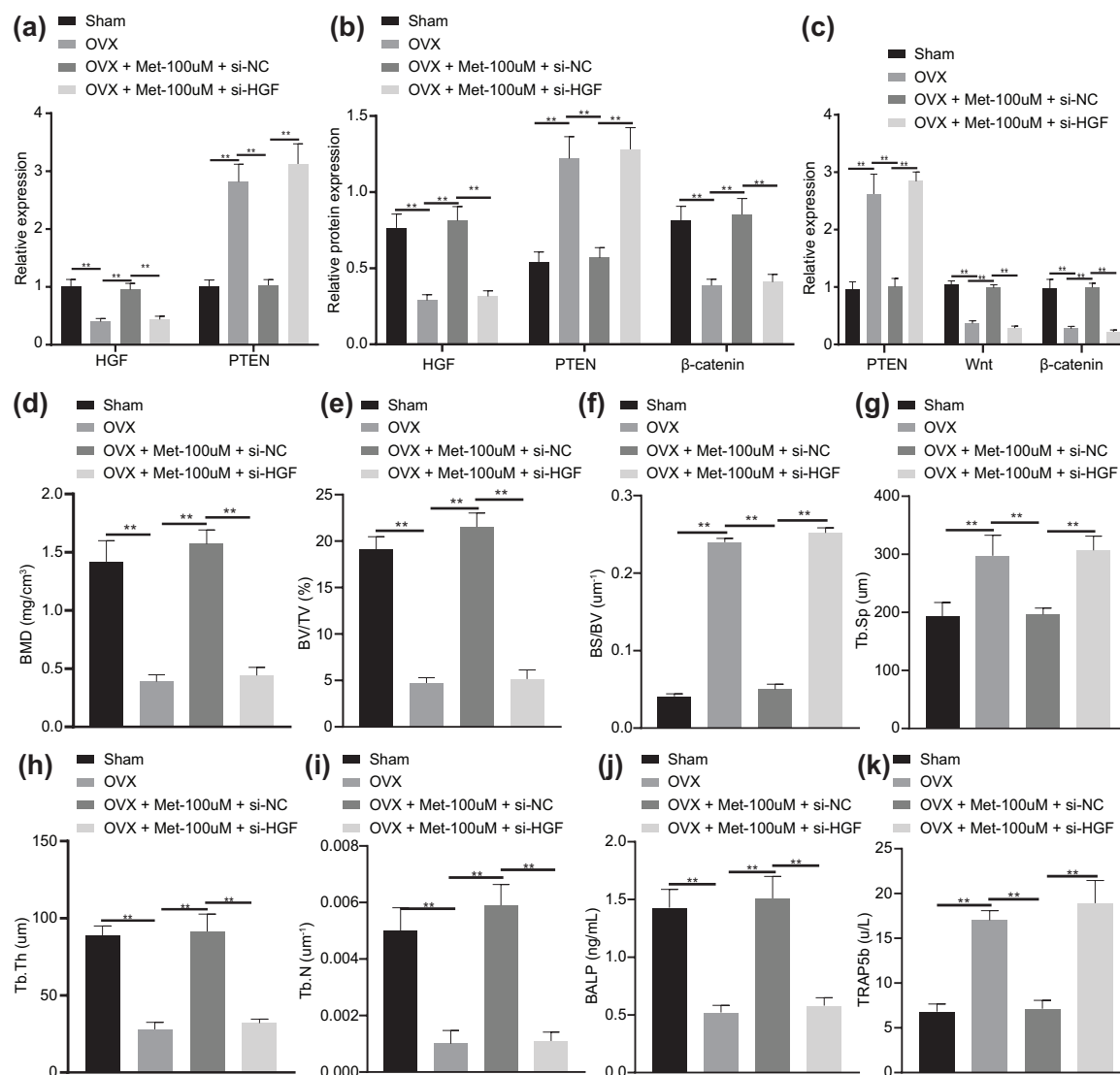
Figure 7. Melatonin delays bone loss and relieves osteoporosis in OVX mice *via* the *HGF*/*PTEN*/*Wnt*/β-catenin axis.
OVX mice were treated with Met-100 μmol/l or in combination with si-*HGF*. (a) mRNA expression of *HGF* and *PTEN* determined by RT-qPCR. (b) Western blot analysis of HGF, PTEN and β-catenin protein expression in OVX mice. (c) Immunohistochemistry analysis of HGF, PTEN and β-catenin proteins. (d) Micro-CT quantitative analysis of BMD in mouse femur. (e) Micro-CT quantitative analysis of BV/TV ratio in mouse femur. (f) Micro-CT quantitative analysis of BS/BV ratio in mouse femur. (g) Micro-CT quantitative analysis of Tb.Sp in mouse femur. (h) Micro-CT quantitative analysis of Tb.Th in mouse femur. (i) Micro-CT quantitative analysis of Tb.N in mouse femur. (j) Serum levels of BALP measured by ELISA. (k) Serum levels of TRAP5b measured by ELISA. $^{**}p < 0.01$, indicates statistical significance. Data (mean ± standard deviation) among multiple groups were compared by one-way ANOVA with Tukey's test. $n = 10$ for mice following each treatment. ANOVA, analysis of variance; ARS, alizarin red S; BALP, bone-specific alkaline phosphatase; BMD, bone mineral density; BMSCs, bone marrow mesenchymal stem cells; BS, bone surface; BV, bone volume; Ca, calcium; CCK, cell-counting kit; CT, computed tomography; Dpd, deoxypridinoline; ELISA, enzyme-linked immunosorbent assay; Met, melatonin; mRNA, messenger ribonucleic acid; OVX, ovariectomy; P, phosphorus; RT-qPCR, real-time qualitative polymerase chain reaction; si-, small interfering; Tb.N, trabecular number; Tb.Sp, trabecular separation; Tb.Th, trabecular thickness; TV, tissue volume.

BALP serum levels and reduced TRAP5b serum levels ($p < 0.01$), which was abolished by subsequent combination with si-*HGF* [$p < 0.01$; Figure 7(j) and

(k)]. The findings suggested that melatonin retarded bone loss and improved osteoporosis in OVX mice *via* the *HGF*/*PTEN*/*Wnt*/β-catenin axis.

Discussion

Osteoporosis results from the imbalance between bone resorption and bone formation, and thus restoring the balance of bone remodeling might be of highest clinical significance in finding treatment options for the disease.[21] Melatonin has been largely reported to participate in the regulation of bone metabolism by controlling the lineage commitment and differentiation pathways of MSCs.[5] Therefore, the current study aimed to explore the potential roles of melatonin in osteogenic differentiation of BMSCs and bone loss following osteoporosis. Both *in vitro* and *in vivo* findings suggested that melatonin could potentially enhance osteogenic differentiation of BMSCs and relieve bone loss *via* the *HGF*/*PTEN*/*Wnt*/β-catenin axis.

We initially found that melatonin attenuated the bone loss in OVX mice. A recent study has revealed the potential of melatonin to prevent the bone loss during space flight, as it significantly stimulates calcitonin (an osteoclast-inhibiting hormone) expression and decreases the expression of receptor activator of nuclear factor κB ligand (a promoter of osteoclastogenesis), alongside suppressed gene expression for osteoclast functions.[22] Moreover, melatonin can alleviate bone loss in the retinoic-acid-induced osteoporosis mouse model, repair the trabecular microstructure, and promote bone formation by reducing oxidation levels *in vivo* and *in vitro via* the *ERK*/*SMAD* and *NF-κB* pathways.[12] Additionally, we uncovered that melatonin could enhance the osteogenic differentiation of BMSCs *in vitro*. Similarly, administration of melatonin stimulates osteoblast differentiation of BMSCs by preserving silent information regulator type 1 (*SIRT1*)-mediated intracellular antioxidant properties.[23] In addition, the research performed by Zhou *et al.*[11] unveiled that melatonin augmented BMSC osteogenic action *via* MT2-inactivated NF-κB pathway. Also, another study uncovered that melatonin enhanced ALP activity and the expression of genes related to osteogenic and chondrogenic differentiation including ALP, osteopontin, osteocalcin, and runt-related transcription factor 2 in human MSCs *via* MT2.[24] Moreover, research conducted by Amstrup *et al.*[25] unraveled that melatonin actions on the skeleton were through effects on calcium excretion and no actions on bone-marker turnover, which warranted further research to explore the potential mechanisms of action of melatonin in bone in the future.

Recently, melatonin has been found to possess atheroprotective effects *via* the upregulation of anti-inflammatory *HGF* in an atherosclerosis rabbit model.[26] *HGF* is a survival factor for BMSCs and the recombinant adenovirus-carrying *HGF* gene can promote human BMSC proliferation and osteogenic differentiation.[27] Additionally, the results from the current study revealed that *HGF* expression was increased in OVX-induced mice. In accordance with our results, serum *HGF* levels are much higher in the ankylosing spondylitis patients compared with the healthy controls, and *HGF* is associated with lower BMD.[28] Taken together, melatonin may have the potency to promote the differentiation of BMSCs into osteoblasts by upregulating transcription factor *HGF*.

In BMSCs exposed to hypoxia, miR-486 elevates *HGF* mRNA and protein levels while inhibiting the *PTEN* expression,[29] suggesting a possible adverse correlation of *HGF* expression with the *PTEN* expression. In addition, *HGF* attenuates transforming growth factor-β-angiotensin II crosstalk through inhibition of the *PTEN*/*Akt* pathway in mice with renal injury.[30] Furthermore, inhibiting the expression of *PTEN* by lncRNA GHET1 contributes to the promoted osteoblast proliferation and differentiation.[31] Treatment with melatonin has the capacity to downregulate the levels of *PTEN* in primary neurons upon Aβ-induced neurotoxicity.[32] Therefore, we concluded that melatonin might enhance the differentiation of BMSCs into osteoblasts *via HGF*-dependent *PTEN* downregulation.

Another important finding in the present study was that knockdown of *PTEN* facilitated activation of the *Wnt*/β-catenin pathway in BMSCs. Consistently, β-catenin activation is revealed to cooperate with *PTEN* deficiency to elicit androgen-receptor-independent castration-resistant prostate cancer.[33] Promoted activity of *PTEN* could suppress the activation of the *Wnt*/β-catenin pathway in HeLa and SW620 cell lines.[34] The augmented *Wnt*/β-catenin pathway activation induced by overexpression of miR-141 can inhibit the osteoporosis of jawbones in OVX-treated rats.[35] LiCl, an activator of the *Wnt*/β-catenin pathway, restores the inhibited osteogenic differentiation by HOXA10 overexpression in human periodontal ligament stem cells.[36] Activated *Wnt*/β-catenin pathway results in an increase in the osteogenic
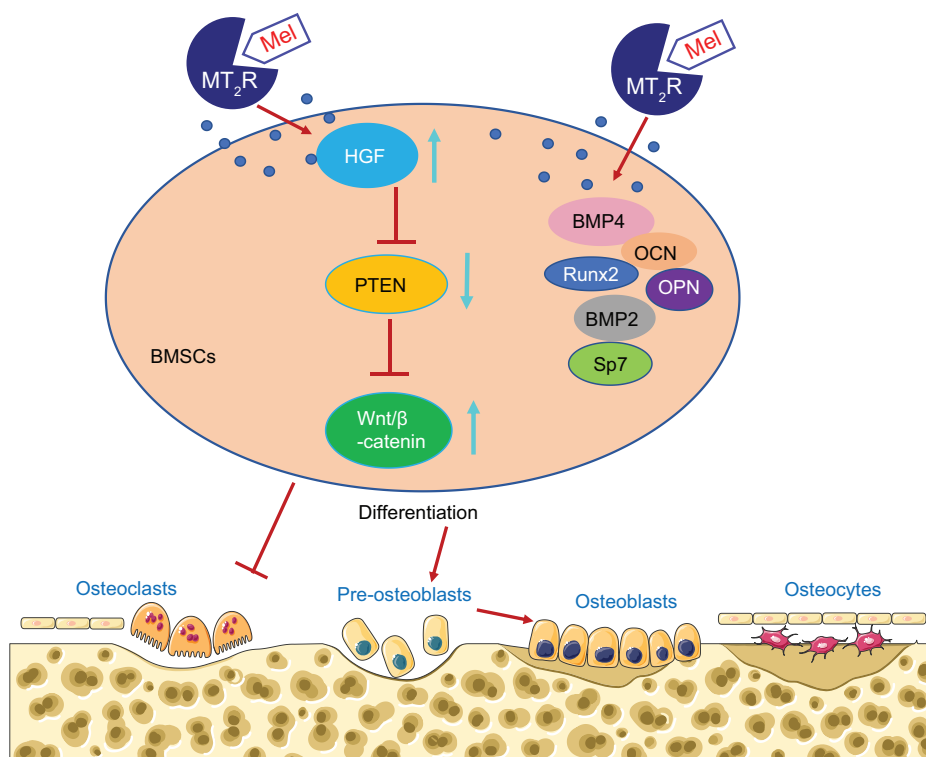
Figure 8. Molecular mechanism underling that melatonin induces osteogenic differentiation of BMSCs and alleviates bone loss *via* the *HGF*/*PTEN*/*Wnt*/β-catenin pathway.
BMSCs, bone marrow mesenchymal stem cells; Mel, melatonin.

differentiation in BMSCs and significantly reduces bone loss by enhancing bone formation in OVX mice.[18] Notably, melatonin promotes osteogenic differentiation in C3H10T1/2 cells partially by activating the β-catenin pathway.[5] On the basis of aforementioned evidence, it can be concluded that melatonin has the potential to elicit osteogenic differentiation in BMSCs, as well as relieving osteoporosis in OVX mice *via* the *HGF*/*PTEN*/*Wnt*/β-catenin pathway.

Conclusion

To conclude, we have demonstrated that melatonin can potentiate osteogenic differentiation and attenuate bone loss *via* the *HGF*/*PTEN*/*Wnt*/β-catenin axis. Melatonin could orchestrate osteogenic differentiation of BMSCs in a receptor-dependent and -independent manner. On the one hand, melatonin upregulates *HGF* and inhibits the expression of *PTEN*, which then activates the *Wnt*/β-catenin signaling pathway. On the other hand, melatonin promotes the osteogenic differentiation of BMSCs by promoting the

expression of BMP4, Runx2, Sp7, OCN, OPN and BMP2 to prevent bone loss (Figure 8). Our data suggest that administration of melatonin is a promising strategy for treating patients with osteoporosis and other related bone-related diseases. However, future studies are still warranted on the specimens from osteoporosis-diagnosed patients for in-depth analysis of the melatonin/*HGF*/*PTEN*/*Wnt*/β-catenin signaling in osteoporosis.

Author contributions
Jun Zhang, Guoliang Jia, Pan Xue and Zhengwei Li designed the study. Jun Zhang and Guoliang Jia collated the data, carried out data analyses and produced the initial draft of the manuscript. Pan Xue and Zhengwei Li contributed to drafting the manuscript. All authors have read and approved the final submitted manuscript.

ORCID iD

Zhengwei Li (iD) https://orcid.org/0000-0002-3795-1016

Availability of data and material

The datasets generated/analyzed during the current study are available.

Supplemental material

Supplemental material for this article is available online.

References

1. Ensrud KE and Crandall CJ. Osteoporosis. *Ann Intern Med* 2017; 167: ITC17–ITC32.

2. Yang HY, Huang JH, Chiu HW, *et al.* Vitamin D and bisphosphonates therapies for osteoporosis are associated with different risks of atrial fibrillation in women: a nationwide population-based analysis. *Medicine (Baltimore)* 2018; 97: e12947.

3. Zhang X, Dai Z, Lau EHY, *et al.* Prevalence of bone mineral density loss and potential risk factors for osteopenia and osteoporosis in rheumatic patients in China: logistic regression and random forest analysis. *Ann Transl Med* 2020; 8: 226.

4. Tang DZ, Hou W, Zhou Q, *et al.* Osthole stimulates osteoblast differentiation and bone formation by activation of beta-catenin-BMP signaling. *J Bone Miner Res* 2010; 25: 1234–1245.

5. Jiang T, Xia C, Chen X, *et al.* Melatonin promotes the BMP9-induced osteogenic differentiation of mesenchymal stem cells by activating the AMPK/β-catenin signalling pathway. *Stem Cell Res Ther* 2019; 10: 408.

6. Wang C, Meng H, Wang X, *et al.* Differentiation of bone marrow mesenchymal stem cells in osteoblasts and adipocytes and its role in treatment of osteoporosis. *Med Sci Monit* 2016; 22: 226–233.

7. Baltatu OC, Amaral FG, Campos LA, *et al.* Melatonin, mitochondria and hypertension. *Cell Mol Life Sci* 2017; 74: 3955–3964.

8. Hastings MH, Maywood ES and Brancaccio M. Generation of circadian rhythms in the suprachiasmatic nucleus. *Nat Rev Neurosci* 2018; 19: 453–469.

9. Sharan K, Lewis K, Furukawa T, *et al.* Regulation of bone mass through pineal-derived melatonin-MT2 receptor pathway. *J Pineal Res* 2017; 63: e12423.

10. Maria S, Samsonraj RM, Munmun F, *et al.* Biological effects of melatonin on osteoblast/osteoclast cocultures, bone, and quality of life: implications of a role for MT2 melatonin receptors, MEK1/2, and MEK5 in melatonin-mediated osteoblastogenesis. *J Pineal Res* 2018; 64: 3.

11. Zhou Y, Wang C, Si J, *et al.* Melatonin up-regulates bone marrow mesenchymal stem cells osteogenic action but suppresses their mediated osteoclastogenesis via MT2-inactivated NF-κB pathway. *Br J Pharmacol* 2020; 177: 2106–2122.

12. Wang X, Liang T, Zhu Y, *et al.* Melatonin prevents bone destruction in mice with retinoic acid-induced osteoporosis. *Mol Med* 2019; 25: 43.

13. Zhu P, Liu J, Shi J, *et al.* Melatonin protects ADSCs from ROS and enhances their therapeutic potency in a rat model of myocardial infarction. *J Cell Mol Med* 2015; 19: 2232–2243.

14. Kong F, Shi X, Xiao F, *et al.* Transplantation of hepatocyte growth factor-modified dental pulp stem cells prevents bone loss in the early phase of ovariectomy-induced osteoporosis. *Hum Gene Ther* 2018; 29: 271–282.

15. Zhu A, Kang N, He L, *et al.* MiR-221 and miR-26b regulate chemotactic migration of MSCs toward HGF through activation of Akt and FAK. *J Cell Biochem* 2016; 117: 1370–1383.

16. Chen Y, Yu H, Zhu D, *et al.* miR-136-3p targets PTEN to regulate vascularization and bone formation and ameliorates alcohol-induced osteopenia. *FASEB J* 2020; 34: 5348–5362.

17. Li Y, Yan X, Shi J, *et al.* Aberrantly expressed miR-188-5p promotes gastric cancer metastasis by activating Wnt/β-catenin signaling. *BMC Cancer* 2019; 19: 505.

18. Shen G, Ren H, Shang Q, *et al.* Foxf1 knockdown promotes BMSC osteogenesis in part by activating the Wnt/β-catenin signalling pathway and prevents ovariectomy-induced bone loss. *EBioMedicine* 2020; 52: 102626.

19. Zeng X, Wang Y, Dong Q, *et al.* DLX2 activates Wnt1 transcription and mediates Wnt/β-catenin

signal to promote osteogenic differentiation of hBMSCs. *Gene* 2020; 744: 144564.

20. Li R and Shen Y. An old method facing a new challenge: re-visiting housekeeping proteins as internal reference control for neuroscience research. *Life Sci* 2013; 92: 747–751.

21. Zhao XL, Chen JJ, Zhang GN, *et al.* Small molecule T63 suppresses osteoporosis by modulating osteoblast differentiation via BMP and WNT signaling pathways. *Sci Rep* 2017; 7: 10397.

22. Ikegame M, Hattori A, Tabata MJ, *et al.* Melatonin is a potential drug for the prevention of bone loss during space flight. *J Pineal Res* 2019; 67: e12594.

23. Chen W, Chen X, Chen AC, *et al.* Melatonin restores the osteoporosis-impaired osteogenic potential of bone marrow mesenchymal stem cells by preserving SIRT1-mediated intracellular antioxidant properties. *Free Radic Biol Med* 2020; 146: 92–106.

24. Chen C, Xu C, Zhou T, *et al.* Abnormal osteogenic and chondrogenic differentiation of human mesenchymal stem cells from patients with adolescent idiopathic scoliosis in response to melatonin. *Mol Med Rep* 2016; 14: 1201–1209.

25. Amstrup AK, Sikjaer T, Mosekilde L, *et al.* Melatonin and the skeleton. *Osteoporos Int* 2013; 24: 2919–2927.

26. Hu ZP, Fang XL, Sheng B, *et al.* Melatonin inhibits macrophage infiltration and promotes plaque stabilization by upregulating anti-inflammatory HGF/c-Met system in the atherosclerotic rabbit: USPIO-enhanced MRI assessment. *Vascul Pharmacol* 2020; 127: 106659.

27. Wen Q, Zhang S, Du X, *et al.* The multiplicity of infection-dependent effects of recombinant adenovirus carrying HGF gene on the proliferation and osteogenic differentiation of human bone marrow mesenchymal stem cells. *Int J Mol Sci* 2018; 19: 734.

28. Torres L, Klingberg E, Nurkkala M, *et al.* Hepatocyte growth factor is a potential biomarker for osteoproliferation and osteoporosis in ankylosing spondylitis. *Osteoporos Int* 2019; 30: 441–449.

29. Shi XF, Wang H, Xiao FJ, *et al.* MiRNA-486 regulates angiogenic activity and survival of mesenchymal stem cells under hypoxia through modulating Akt signal. *Biochem Biophys Res Commun* 2016; 470: 670–677.

30. Iekushi K, Taniyama Y, Kusunoki H, *et al.* Hepatocyte growth factor attenuates transforming growth factor-β–angiotensin II crosstalk through inhibition of the PTEN/Akt pathway. *Hypertension* 2011; 58: 190–196.

31. Li D, Li L, Chen X, *et al.* LncRNA GHET1 promotes osteoblast proliferation and differentiation by inhibiting PTEN. *Panminerva Med*. Epub ahead of print 29 July 2019. DOI: 10.23736/S0031-0808.19.03701-7.

32. Zhao Y, Zhao R, Wu J, *et al.* Melatonin protects against Aβ-induced neurotoxicity in primary neurons via miR-132/PTEN/AKT/FOXO3a pathway. *Biofactors* 2018; 44: 609–618.

33. Patel R, Brzezinska EA, Repiscak P, *et al.* Activation of β-catenin cooperates with loss of Pten to drive AR-independent castration-resistant prostate cancer. *Cancer Res* 2020; 80: 576–590.

34. Lu D, Zhou Y, Li Q, *et al.* Synthesis, in vitro antitumor activity and molecular mechanism of novel furan derivatives and their precursors. *Anticancer Agents Med Chem* 2020; 20: 1475–1486.

35. Liu TJ and Guo JL. Overexpression of microRNA-141 inhibits osteoporosis in the jawbones of ovariectomized rats by regulating the Wnt/β-catenin pathway. *Arch Oral Biol* 2020; 113: 104713.

36. Wang C, Li Y, Yu K, *et al.* HOXA10 inhibit the osteogenic differentiation of periodontal ligament stem cells by regulating β-catenin localization and DKK1 expression. *Connect Tissue Res*. Epub ahead of print 27 April 2020. DOI: 10.1080/03008207.2020.17562711-9.